AFRL-RX-WP-TP-2009-4211

COARSENING KINETICS OF γ' PRECIPITATES IN THE COMMERCIAL NICKEL BASE SUPERALLOY RENE88DT (PREPRINT)

J. Tiley, G.B. Viswanathan, R. Srinivasan, R. Banerjee, D.M. Dimiduk, and H.L. Fraser

Metals Branch
Metals, Ceramics, and NDE Division

SEPTEMBER 2008

AIR FORCE RESEARCH LABORATORY
MATERIALS AND MANUFACTURING DIRECTORATE
WRIGHT-PATTERSON AIR FORCE BASE, OH 45433-7750
AIR FORCE MATERIEL COMMAND
UNITED STATES AIR FORCE

REPORT DOCUMENTATION PAGE

Form Approved
OMB No. 0704-0188

1. REPORT DATE *(DD-MM-YY)*	2. REPORT TYPE	3. DATES COVERED *(From - To)*
September 2008	Journal Article Preprint	

4. TITLE AND SUBTITLE

COARSENING KINETICS OF γ' PRECIPITATES IN THE COMMERCIAL NICKEL BASE SUPERALLOY RENE88DT (PREPRINT)

5a. CONTRACT NUMBER
In-house

5b. GRANT NUMBER

5c. PROGRAM ELEMENT NUMBER
62102F

6. AUTHOR(S)

J. Tiley and D.M. Dimiduk (AFRL/RXLMD)
G.B. Viswanathan, R. Srinivasan, and H.L. Fraser (The Ohio State University)
R. Banerjee (University of North Texas)

5d. PROJECT NUMBER
4347

5e. TASK NUMBER
RG

5f. WORK UNIT NUMBER
M02R1000

7. PERFORMING ORGANIZATION NAME(S) AND ADDRESS(ES)

Metals Branch (AFRL/RXLMD)
Metals, Ceramics, and NDE Division
Materials and Manufacturing Directorate
Wright-Patterson Air Force Base, OH 45433-7750
Air Force Materiel Command, United States Air Force

The Ohio State University
Dept. of Materials and Engineering
Columbus, OH 43210

University of North Texas
Dept. of Materials Science & Engineering
Denton, TX 76203

8. PERFORMING ORGANIZATION REPORT NUMBER
AFRL-RX-WP-TP-2009-4211

9. SPONSORING/MONITORING AGENCY NAME(S) AND ADDRESS(ES)

Air Force Research Laboratory
Materials and Manufacturing Directorate
Wright-Patterson Air Force Base, OH 45433-7750
Air Force Materiel Command
United States Air Force

10. SPONSORING/MONITORING AGENCY ACRONYM(S)
AFRL/RXLMD

11. SPONSORING/MONITORING AGENCY REPORT NUMBER(S)
AFRL-RX-WP-TP-2009-4211

12. DISTRIBUTION/AVAILABILITY STATEMENT
Approved for public release; distribution unlimited.

13. SUPPLEMENTARY NOTES
Journal article submitted to *Acta Materialia*. PAO Case Number: WPAFB 08-5199; Clearance Date: 25 Aug 2008.

14. ABSTRACT

Rene88DT samples were subjected to different cooling rates after a supersolvus treatment, and aged for varying periods of time from 25 to 200 hours at 760 °C. Secondary and tertiary γ' precipitate sizes were measured after each heat treatment condition through scanning electron microscopy (SEM) and energy filtered transmission electron microscopy (EFTEM). Coarsening rate constants were calculated and reported from the measured values of precipitate sizes. When describing the change in radius (r) as a function of time (t), good fits between the experimental results and analysis resulted from the use of both types of functional relationships, r^3 vs. t and r^2 vs. t. The experimental rate constants derived from this analysis were compared with theoretical values deduced from two different models - volume diffusion and interface-controlled diffusion. The mechanism for γ'coarsening has been rationalized based upon the comparison between the analytically derived and experimentally observed values, of these rate constants.

15. SUBJECT TERMS
Rene88DT, nickel base superalloy, coarsening, scanning electron microscope, energy filtered transmission electron microscopy

16. SECURITY CLASSIFICATION OF:			17. LIMITATION OF ABSTRACT:	18. NUMBER OF PAGES	19a. NAME OF RESPONSIBLE PERSON (Monitor)
a. REPORT	b. ABSTRACT	c. THIS PAGE			Christopher F. Woodward
Unclassified	Unclassified	Unclassified	SAR	32	19b. TELEPHONE NUMBER *(Include Area Code)* N/A

Standard Form 298 (Rev. 8-98)
Prescribed by ANSI Std. Z39-18

Coarsening Kinetics of γ' Precipitates in the Commercial Nickel base Superalloy Rene88DT

J. Tiley[1], G.B. Viswanathan[2], R. Srinivasan[2], R. Banerjee[3], D.M.Dimiduk[1] and H.L. Fraser[2]

[1]Materials and Manufacturing Directorate, Air Force Research Laboratory, Dayton OH
[2]Department of Materials and Engineering, The Ohio State University, Columbus OH 43210
[3]Department of Materials Science and Engineering, University of North Texas, Denton TX 76203

Abstract

Rene88DT samples were subjected to different cooling rates after a supersolvus treatment, and aged for varying periods of time from 25 to 200 hours at 760^{0}C. Secondary and tertiary γ' precipitate sizes were measured after each heat treatment condition through Scanning Electron Microscopy (SEM) and Energy Filtered Transmission Electron Microscopy (EFTEM). Coarsening rate constants were calculated and reported from the measured values of precipitate sizes. When describing the change in radius (r) as a function of time (t), good fits between the experimental results and analysis resulted from the use of both types of functional relationships, r^3 vs. t and r^2 vs. t. The experimental rate constants derived from this analysis were compared with theoretical values deduced from two different models – volume diffusion and interface-controlled diffusion. The mechanism for γ' coarsening has been rationalized based upon the comparison between the analytically derived and experimentally observed values, of these rate constants.

1. Introduction

Rene88DT is a commercial Nickel-base superalloy used in the high temperature section of aerospace propulsion systems. It is typically subjected to a two-stage supersolvus heat treatment: the material is first solutionized by heating above the solvus, and then cooled to precipitate an $L1_2$ ordered Ni_3Al precipitate (secondary γ') from the FCC matrix (γ). The cooling rate determines the size and distribution of the precipitates. The second heat treatment step involves aging the material to precipitate a refined dispersion of ordered tertiary γ' precipitates. The tertiary γ' is more or less spherical and has an effective particle size much smaller then the secondary γ'. As documented in numerous studies, the morphology and size of the precipitates greatly impact the mechanical properties of the materials [1-3]. Precipitate-matrix interaction, influenced in part by the lattice parameter misfit between the ordered precipitates and the matrix, combined with the size and volume fraction of the precipitates, has been reported to affect properties such as creep behavior [4-6] in these alloys.

Several other aspects related to the composition and morphology of the γ' precipitates, including the chemical gradients across γ / γ' interfaces, have also been discussed as contributing factors to precipitate coarsening [7,8]. Overall the morphologies and mechanisms associated with γ' particle coarsening with aging have been a topic of significant discussion over the past decades [9-15]. The theories and Lifshitz and Slyozov [9] and Wagner [10], known collectively as the

LSW theory, predict the coarsening of dispersed particles in a matrix to follow the general relationship $r^3 = kt$, where r denotes the particle radius, t denotes the aging time and k denotes the rate constant associated with coarsening. Other modifications have been proposed, to account for some of the assumptions involved with the LSW theory [16]. In contrast, recently Ardell and Ozolins [17] have proposed a new model, based upon interface diffusion, to account for the coarsening of the γ' precipitates in superalloys. They have argued that the fundamental assumptions of the LSW theory are valid only under certain restrictive conditions which may not apply directly to the case of γ' coarsening in superalloys.

While significant experimental evidence is in fact available on the subject of γ' coarsening and growth in Nickel-base superalloys, the goal of this study is to provide a comprehensive study of γ' (secondary and tertiary) size evolution over various cooling rates and aging times for Rene88DT. Additionally, not much information exists on the actual rate constants associated with coarsening in Rene88DT, and the effect of initial microstructures on the coarsening kinetics. Hence, this study focuses on the determination of rate constants in Rene88DT for the two different mechanisms proposed (a) volume diffusion, based on the LSW model [9,10], and (b) interface diffusion driven mechanism based on the model proposed by Ardell and Ozolins [17]. Size measurements of γ' precipitates have been made through the use of back scattered SEM and energy filtered transmission electron microscopy (EFTEM) techniques. The measured sizes have been plotted as a function of cooling rate and aging time, to determine the actual rate constants associated with γ' growth/coarsening, as a function of aging time and cooling rate. These values are compared with those measured previously in similar systems, and also compared with theoretically derived rate constants based on the two different models. Finally, the mechanism of γ' coarsening has been rationalized, based upon these comparisons.

2. Experimental Procedures

The bulk chemical composition of Rene88DT is provided in **Table 1**. Material was cut from the bore and rim section of a disk, produced and tested under work supported by the Defense Advanced Research Projects Agency, Defense Sciences Office (Engine Systems Prognosis, Contract Nos. HR0011-04-C-0001 and HR0011-04-C-0002). ~~The program evaluated the impact of microstructure on mechanical properties [18].~~ The samples were supersolvus solution treated at 1150^{0}C for 30 minutes to dissolve primary γ and then cooled under one of three cooling rates – slow cooled (SC) at 24^{0}C/min, fast cooled (FC) at 280^{0}C/min and water quenched (WQ) at a rate >300^{0}C/min. The FC and SC samples were solutionized in a large vacuum chamber. Water quenched samples were drilled to accommodate a thermocouple in the center of the sample. They were heated in a non-vacuum furnace to allow for rapid water quenching of the material. Despite these elaborate procedures, it is expected that the water quenched samples cooled at a rate faster than the rate relayed by the thermocouple to the data acquisition system.

Following cooling, the samples were aged for 25, 50, 100 and 200 hours respectively, at a temperature of 760^{0}C, in a vacuum furnace equipped with a large chamber and air quenched. Following aging, the samples were cut and polished for wavelength dispersive spectroscopy (WDS) homogeneity analysis using a Cameca SX 100 microprobe. Each of the samples was evaluated for all of the chemical elements present in the bulk chemistry data by averaging 100 points in a line scan with a 5 μm defocused probe operating at 15 kV.

Standard metallographic processes were used to mount and polish scanning electron microscopy samples for back scattered SEM, performed using a FEI Sirion field emission gun SEM operated at 10 and 15 kV. Prior to imaging, samples underwent various treatments to elucidate γ' precipitate morphology with limited detrimental etching of features. Even with additional processing controls, measurement results were subject to errors based on the flatness of the image surface and the etching of precipitates and/or matrix material. Because of the forging history of the disk material, the γ texture of the samples was evaluated using orientation imaging microscopy of a fast cooled, un-aged specimen. The analysis was performed at 20kV, with a step size of 1 μm and a probe spot size of 3 over an area of 1.9 mm^2.

For Transmission Electron Microscopy (TEM) investigations, samples were cut using diamond saws, polished to 100 μm thickness, and core-drilled to produce 3 mm diameter discs. Thin foils for TEM investigation were prepared by dimpling and ion milling of discs, performed on a Fischione Model 1010 ion milling system operating at 6 kV and 5 mA. TEM analysis was conducted on a FEI Tecnai F20 field emission gun transmission electron microscope operating at 200 KV. Images were obtained using the Cr M-edge in the energy filtered TEM (EFTEM) mode, as described elsewhere [7,8]. Images were captured at different magnifications to identify the relevant secondary and/or tertiary γ' precipitates and processed using Fovea Pro [19] and Adobe Photoshop [20] to isolate each precipitate and determine the area fraction from the image pixels. Details of the image stereology analysis are presented elsewhere [21,22]. The area fractions were converted to equivalent diameter values. While this technique provided a straightforward method for comparing precipitate area fractions, it is likely to be a more accurate representation of sizes for smaller precipitates (~3-50 nm) with near-spherical morphologies, as compared to larger (>200 nm) precipitates showing non-spherical morphologies (discussed in detail below).

For 3D Atom Probe (3DAP), specimens were prepared with a tip radius of approximately 50 nm. Specimens were first cut by electro-discharge machining (EDM), followed by electropolishing and Focused Ion Beam (FIB) milling to achieve the fine tip radius required for investigations. All 3DAP experiments were conducted on a LEAP 3000 Local Electrode Atom Probe (LEAP^{TM}) microscope system manufactured by Imago Scientific Instruments, Inc. Additionally, all atom probe experiments were carried out in the electric-field evaporation mode at a temperature of 70K, with the evaporation rate varying from 0.2 – 1.0 % and the pulsing voltage at 30% of the steady-state applied voltage. More details of the sample preparation technique for the 3DAP studies can be found elsewhere [23].

3. Results

A. Composition, texture and volume fraction of precipitates

Compositional determination using WDS confirmed good overall uniformity in samples for a given cooling rate and aging condition. Texture measurements provided a value of 2.53 times random, indicating only a slight texturing of the material. Thus, compositional inhomogeneity and sample texture are not expected to be significant factors influencing γ' precipitate size and

morphology. While the WQ series of samples exhibited near-spherical morphologies and a unimodal size distribution of γ' precipitates for all aging times, the FC and SC series of samples exhibited a bimodal size distribution of precipitates with distinctly different morphologies. Thus, while the smaller precipitates in the FC and SC samples were found to be near-spherical, the larger precipitates tended to exhibit more cuboidal-like morphologies. Subsequently in this paper, the larger γ' precipitates in the FC and SC samples as well as all the precipitates in the WQ samples will be referred to as secondary γ' and the smaller precipitates in the FC and SC samples will be referred to as tertiary γ',.i.e., for the purpose of this study, a distinction is made (in SC and FC samples) between secondary and tertiary γ' purely based on the precipitate sizes. Volume fraction measurements conducted on backscatter SEM images of slow cooled samples yielded a reasonably consistent value in the range of 32.1 % to 34.1% (for secondary γ') over the aging range from 0 hours to 200 hours. Volume fractions for tertiary γ' precipitates, measured from slow cooled, 200 hour aged as well as electropolished samples (that provided a clear distinction of γ/γ' interfaces) yielded a value of 9.7%. Thus, an approximate γ' volume fraction of 41-43% was measured, in reasonable agreement with previous measurements reported for Rene 88DT [24].

B. Measurement of Equivalent Diameters

As mentioned above, SEM imaging was done selectively, primarily to image larger γ' precipitates in the slow-cooled samples. For samples with smaller precipitates (tertiary γ', fast cooled and water quenched samples), use of ultra-high resolution and back-scattered SEM techniques did not yield marked improvements in image contrast and quality. Consequently, EFTEM was used to image the γ' precipitates effectively. As illustrated in the representative EFTEM images shown in Figure 1 (before aging) and Figure 2 (after aging for 200 hours), both secondary and tertiary γ' precipitate boundaries were clearly identifiable for all aging conditions. WQ samples showed a unimodal particle size distribution, with spherical γ' morphology. For FC and SC specimens, exhibiting a bimodal size distribution, lower magnification images (typically 18500X magnification) were used to determine the area fractions of the larger (primarily secondary) γ' precipitates, which expectedly become less spherical with increasing aging time [25]. Higher magnifications (typically 71000X or 135000X) were used to image the spherical (primarily tertiary) γ' precipitates. Size measurements were made for at least 250 particles in each case. The errors in the sample data sets were determined using the equation below [26]:

why would you expect this?

$$S.E. = s / (N)^{0.5} \qquad (1)$$

where S.E. is the standard sample error, s is the standard deviation over all measurements in a sample, and N is the number of measurements. Given the large number of measurements, the errors were insignificant, except for the case of secondary γ' precipitate sizes for SC samples (discussed below).

Several simple observations can be made from the observed results, as below:

a) The equivalent diameters for the un-aged secondary γ' precipitates increased with decreasing cooling rates (WQ0 < FC0 < SC0).

b) Equivalent diameters for secondary γ' precipitates increased for all cases with increasing aging time.
c) While the morphology of tertiary γ' precipitates remained near-spherical at all aging times, secondary γ' morphology became increasingly non-spherical and more cuboidal-like with increasing aging time. to me it started cuboidal and became more convoluted
d) Volume fractions calculated from EFTEM images remained roughly constant for all samples, as a function of aging time.

The above observations are important as a systematic experimental study of the coarsening behavior of γ' precipitates in Rene88DT. It is worth mentioning that a more detailed understanding of the size evolution during short aging periods (0-25 hours) forms part of a separate study [27].

EFTEM images (Figure 1 and Figure 2) show that the secondary γ' morphology becomes increasingly non-spherical with (a) decreasing cooling rates, and (b) increasing aging times ~~at~~ after a given cooling rate, especially for the FC and SC samples. Although the secondary γ' precipitates may coarsen into larger cuboidal-like shapes, the sampling of the structures may create more spherical features of smaller dimension due to the nature of the sampling plane cutting through the precipitate. Consequently, the EFTEM imaging may underestimate the area fraction of the non-spherical structures, as several of these features are expected to be greater than the foil thickness. While some amount of overestimation in sizes may occur for the secondary γ' precipitates due to the projection of the features onto the image plane (mainly due to particles and shapes that may reside in close proximity in three dimensions), this is expected to be relatively small. Consequently, all size values should be treated as a lower bound for the actual sizes of the secondary γ' precipitates. The difference between true and measured values is expected to be much lower for the tertiary γ' precipitates, as these are usually confined within the foil thickness.

not really

this is NOT cuboidal

Figure 3 shows the evolution of precipitate sizes (measured in the form of an equivalent diameter) with aging time for three cases: WQ samples (where a unimodal size distribution is observed), tertiary γ' precipitates in FC samples and tertiary γ' precipitates in SC samples. Note that with increasingly non-spherical shapes being observed in the case of secondary γ' precipitates in FC and SC samples, the concept of an equivalent diameter may not be particularly appropriate, and may in fact yield erroneous values for coarsening rates. The importance of using the correct precipitate morphology and size for determining coarsening kinetics is discussed in more detail below, and has also been addressed in other studies [17].

C. Measurement of solute concentrations and compositional gradients at γ/γ' interface

The solute concentrations in the γ and γ' phases and the compositional gradient across the γ/γ' interface have been determined using 3D atom probe tomography studies. As an example, Figure 4 shows the results of 3DAP studies carried out on the WQ50 sample. Figure 4(a) shows a 3D reconstruction of the Al=8at% iso-concentration surface (in red) corresponding to the γ' precipitates together with the Co atoms plotted in blue. Figure 4b shows the same 3D atom probe reconstruction with the Cr=14at% iso-concentration surface plotted to define the γ' precipitates. Finally in Figure 4(c), the concentration profiles of various alloying elements across the γ/γ'

interface have been plotted for a specific tertiary precipitate (marked by the arrow in Figure 4(b). The concentration profiles have been determined using the proximity histogram approach wherein the composition of each alloying element at a particular location is plotted as a function of its proximity to the interface [28]. From Figure 4(c) it is evident that while Cr, Co, and, Mo tend to partition strongly to the γ matrix, Al and Ti partition to the γ' precipitate. Furthermore, there appears to be a compositional gradient at the γ/γ' interface, defined as the zero location on the distance axis. The width of this compositional gradient is approximately 3.5 nm for Cr (the major alloying element in Rene 88DT) and this value has been assumed to be the *compositional width* of the interface for use in the coarsening models to be discussed below.

4. Discussion

A. γ' sizes, volume fraction and morphology

As shown in Figure 3, the γ' precipitate sizes are observed to increase with decreasing cooling rate, and increasing aging time. The measured sizes are in agreement with those reported in previous studies on Rene 88DT [7,24]. Similarly, the overall volume fractions of γ' measured in this study are generally in agreement with those reported earlier [24]. The change in size and morphology of secondary γ' precipitates as a function of cooling rate is typical of Ni-base superalloys. In the initial stages of nucleation and growth, the γ' precipitates exhibit a spherical morphology, as observed in the as-cooled microstructures (Figure 1(a)), dictated by the minimization of surface energy per unit volume. While the observed increase in size with slower cooling (due to growth kinetics) is accompanied by significant chemical partitioning, this increase in precipitate size is also accompanied by a change in precipitate morphology; there is a tendency for precipitates to become more cuboidal at lower cooling rates (Figures 1(b) and 1(c)). This is attributed to the rapidly increasing coherency strain energy accompanying the growth and coarsening process. Additionally, significant degree of particle coalescence is ~~also observed~~ suspected at slower cooling rates (FC and SC samples). Consequently, it becomes difficult to attribute the increase in size during aging to simply coarsening processes. Thus, for the purpose of comparison with coarsening models (discussed below), it is important to carefully select morphologies that do not exhibit coalescence effects and retain their near spherical shapes for the most part.

Similar effects are seen during the aging treatment as well. While the precipitates in the WQ sample microstructure tend to be nearly spherical even after 200 hours of aging, the precipitates in the FC and SC samples have a propensity to become cuboidal and ~~more~~ often take on ~~assume~~ arbitrary shapes as shown in Figure 2(b), 2(c) and Figure 5(a). Splitting of coarse γ' precipitates (observed primarily in SC and FC samples aged at 200 hours) into a number of small particles or cuboids has been experimentally observed to occur in other Ni-base alloys [25], and has also been observed in very coarse secondary γ' precipitates in the SC samples subjected to 200 hours of aging, as shown in Figure 5(b). It is important to note that this splitting is not expected to significantly affect the size measurements of the tertiary γ' precipitates in the FC and SC samples, as these tertiary γ' particles have a nearly spherical morphology, and have smaller size ranges (~ 35-40 nm). This is evident through a qualitative comparison of the sizes of the secondary and tertiary γ' particles in Figure 5(a) and 5(b).

Jay, here you talk about possible splitting. In the paragraph before you indicate possible particle coalescence. You are all over the map here. Which is it?

Due to all the factors listed above, it is clear that for the purpose of comparison with coarsening models (discussed below), it is important to select near-equilibrium morphologies that do not exhibit coalescence or splitting effects (as observed in **Figure 5b**). A careful scrutiny of various morphologies suggests that the WQ samples show minimal tendency for coalescence of γ' precipitates, while maintaining a nearly spherical morphology. Similarly, the tertiary γ' precipitates in FC and SC samples also exhibit nearly spherical γ' precipitates and do not typically appear to be coalescing. More importantly, these respective types of γ' precipitates in all three samples lie in the size range of ~3-40 nm, permitting the modeling of coarsening kinetics of these precipitates. Hence, for the purpose of calculating rate constants associated with coarsening, these specific morphologies have been chosen, and discussed below. Note that while the underlying mechanism of coarsening for larger secondary and smaller tertiary γ' precipitates may be the same, the largely non-spherical morphologies of the secondary precipitates coupled with the increased tendency for coalescence and splitting make it rather difficult to apply standard coarsening models. In addition, it is important to note that 3D atom probe studies have indicated some non-uniformity in the composition of individual tertiary γ' precipitates [23,29], especially during the initial stages of growth (precipitate size < 5-10 nm). Consequently, the data points of average γ' sizes in WQ, FC, and, SC samples, prior to aging, are not included in the analysis of the coarsening models as it is likely that the precipitates in these samples are still in the "growth" regime and have not yet entered the "coarsening" regime of the phase transformation.

good.

B. Modeling the coarsening kinetics of γ' precipitates

(i) Classical Lifshitz-Slyozov-Wagner (LSW) coarsening model

The respective γ' precipitates in all three samples, (WQ secondary, FC tertiary and SC tertiary), all exhibit an initial rapid increase with aging time that tapers off at longer aging periods (as illustrated in Figure 3). It has been commonly proposed that coarsening of the γ' precipitates in Ni base superalloys occurs via Ostwald ripening for which theoretical understanding has been extensively developed ~~in the past~~. In case of Ostwald ripening, the rate of mass transport (.i.e. the product of diffusivity and concentration of solute in the matrix) is considered ~~as the~~ rate-limiting ~~step~~ during the coarsening of the precipitates. Typically, such a time dependent coarsening process is described according to the LSW theory by the following power law expression [9,10]:

$$\bar{r}_t^3 - \bar{r}_0^3 = k^v t \qquad (2)$$

extra space

where $\bar{r}_t$ is the mean particle size at a time t, $\bar{r}_0$ is the mean particle size at the onset of coarsening (at $t=0$), and k^v is described as the coarsening constant that is largely dependent on factors such as the volume fraction and size distribution of precipitates. Experimentally the values are obtained from the slope of the plot $\bar{r}_t^3 - \bar{r}_0^3$ versus t. More recent modifications [11,12,16] to the LSW theory continue to use the original power law form of coarsening kinetics expressed by Equation 2 with differing k^v values. Consequently, the power law equation expressed by Equation 2 has been applied to the coarsening behavior of precipitates in all three sets of samples, WQ secondary, FC tertiary, and, SC tertiary, as shown in Figure 6, where the measured precipitate sizes (or equivalent radius raised to the third power), r^3, is plotted as a

? what? k^v is not a constant in [11,12,16]? Explain.

function of the aging time t. Values of the coarsening constant (k^3) are obtained from the slopes of these curves. As mentioned earlier, for the purpose of obtaining rate constants, the data points for samples prior to aging ($t=0$) have not been considered. The WQ sample aged for 200 hours has also not been considered, as there is likely to be interaction of elastic strain fields between larger particles [17], and also particles may not have equilibrium shapes in this regime.

In general, the experimental data of r^3 vs. t appears to fit quite well to the classical LSW coarsening model expressed by Equation 2 for all samples analyzed. The k values obtained from the slopes of these plots are listed in Table 2, and lie in the range 0.0046 to 0.0157 nm^3s^{-1}. Although k values for multi-component superalloys are not widely available in the published literature, these values are closer to those reported in various ternary alloys [12,15]. One of the primary reasons underlying the fact that the k values for the three types of samples all lie within a limited range could be the initial microstructure. Thus, the secondary γ' precipitates in the WQ samples and the tertiary γ' precipitates in the FC and SC samples, chosen for this analysis, have a mono-modal precipitate size distribution similar to the ones in the Ni-Cr-Al alloy studied by Chellman and Ardell [12]. In both studies, the precipitate morphologies are nearly spherical and similar in size range (< 30 nm) prior to aging. Another very important point of similarity to be noted is that both are low misfit alloys ($\delta < 0.05$). Finally, in both these studies minimal coalescence of precipitates has been observed (as compared with the SC and FC secondary precipitates in the present study).

In the classical LSW model of coarsening, the rate constant k depends on a number of parameters including the diffusivity of the solute in the matrix, the solute concentration, as well as the interfacial energy between the matrix and the precipitate. An analytical expression for the rate constant is given below [11,12,15,30]:

$$k = \frac{A.D.C_e.\gamma_i.V_m}{RT}.10^{27} \qquad (3)$$

where D is the diffusion coefficient of solute in the matrix (m^2s^{-1}), C_e is the atomic fraction of solute in equilibrium with the precipitate, γ_i is the precipitate/matrix interface energy, V_m is the molar volume of the precipitate (m^3 mol^{-1}), R is the universal gas constant (J $mole^{-1}$-K^{-1}) and T is the absolute temperature (K). A is a constant dependent on the precipitate distribution in the matrix. k in this equation is expressed in nm^3s^{-1}.

Assuming the equilibrium solute concentration does not vary with aging temperature, i.e. C_e/T remains constant in **Equation 3**, the activation energy for coarsening can be obtained by plotting log(k) vs. 1/T. Studies conducted on various binary and ternary Ni-base superalloys have reported activation energy values in the range of 260-280 J/mole-K [31]. These values are closer to the activation energy for Al diffusion in Ni, consistent with the volume diffusion mechanism suggested for γ' precipitate coarsening in Ni-base superalloys [32]. Recent studies by Isheim et al. [33] in model Ni-Cr-Al alloys with refractory metal additions, have also shown the Al concentration in the γ' precipitates to vary inversely with increasing aging time, lending added support to this argument.

The rate constant (k) for the aging of γ' precipitates for the WQ microstructures has been calculated using **Equation 3** and the following parameters: A = 8/9 [30], diffusivity for Al diffusion in Ni at 1033K = 7 x 10^{-18} m^2s^{-1} [34], interface energy, γ_i = 0.0037 Jm^{-2} [17], gas constant R=8.31 J mole-K^{-1}, molar volume of the precipitate V_m= 2.716 x 10^{-5} m^3 mol^{-1} [15] and aging temperature T = 1033K (760^0C).

While the parameters discussed above are available in the literature, the value of the solute concentration C_e is specific to the alloy and aging condition. In the past various experimental methods have been used to obtain the solute concentration C_e in the γ matrix. Chellman and Ardell [12] used the Curie temperature calibration method to arrive at the solute content of the matrix. Others have used more conventional X-ray spectroscopy in the TEM [24,25]. In this study, solute content of the γ matrix was accurately determined from the heat-treated sample using 3D atom probe (3DAP) studies, as shown in Figure 4. Thus the value of C_e for Al was taken as 0.03 (3 at%).

Substituting these various values into Equation 3, a value of k = 0.002 nm^3s^{-1} was obtained. This value is only marginally lower than the range of experimentally determined k values reported in Table 2. Interestingly, the study by Isheim et al. [33] on Ni-Cr-Al model systems has shown the time constant for r vs. t to be near 3 regardless of alloying additions and elastic strain energies (indicative of cuboidal γ' precipitates).

Noting that for Rene 88DT, the primary alloying addition is Cr, it can be argued that the Cr diffusivity in the γ phase could constitute the rate limiting step in the coarsening process. Taking the diffusivity of Cr in Ni at 1033K to be 1.8x10^{-18} m^2s^{-1} [34], C_e for Cr as 0.3 from the 3D atom probe data [23], and keeping the other parameters the same as discussed above, the rate constant, k, is calculated to be 0.005 nm^3s^{-1}. This value of k is in good agreement with the experimentally determined range listed in Table 2, considering the significant assumptions involved in the calculation, especially with respect to values of the various parameters (such as the γ/γ' interfacial energy) that are not well known for a complex multicomponent alloy such as Rene 88.

(ii) *Trans-interface diffusion-controlled (TIDC) coarsening model (Ardell and Ozolins)*

Ardell and Ozolins [17] have recently proposed a model based on the notion that the rate-limiting step associated with the coarsening of γ' precipitates in a γ matrix is the diffusion of solute elements through the order-disorder γ/γ' interface. In such a scenario, the particle size evolution with aging time has been proposed to follow a behavior as shown below:

$$\bar{r}_t^2 - \bar{r}_0^2 = k^i t \qquad (4)$$

where k^i is the coarsening constant based upon an interface diffusion controlled mechanism, and has units of nm^2s^{-1}. Figure 7 shows the plot of the square of measured particle sizes (or equivalent radius, as in this study), r^2, vs. the aging time (t). The experimental data points have been fitted to a linear function with excellent R^2 values, comparable to the R^2 values obtained in case of the fitting of the r^3 vs. the aging time (t) data shown in Figure 6. The coarsening constant, k^i values, are listed in Table 3.

The rate constant for the TIDC model can be analytically expressed by the following expression [17]:

$$k^{i} = \frac{32\tilde{D}_i l_\gamma}{81\Delta X_e \delta} 10^{18} \quad (5)$$

where $\tilde{D}_i$ is the trans-interface diffusion coefficient, l_γ is the capillary length, $\Delta X_e = X_\gamma - X_{\gamma'}$ is the difference in solute concentration between the equilibrium compositions of the precipitate and matrix, δ is the interface width, and k^i is the coarsening constant having units of nm^2s^{-1}. The capillary length is calculated using the following equation [17]:

$$l_\gamma = \frac{2V_m^* \gamma}{\Delta X_e G''_{m\gamma}} \quad (6)$$

where V_m^* is the partial molar volume of the element under consideration in the γ' phase and $G''_{m\gamma}$ is the local curvature of the molar free energy of mixing of the γ phase, calculated at the composition X_γ. *In the present calculation, the value of* $G''_{m\gamma}$ was calculated using the expression given by Calderon et al. [30] for $X_\gamma = 0.03$ *(corresponding to Al).*

Using the 3D atom probe experimental values for Al (refer Figure 4) $\Delta X_e = 0.08$, $\delta = 3.5$ nm for the interface width, and $X_{\gamma} = 0.11$, and a value of $k^i = 0.0006\ nm^2s^{-1}$ obtained from the slope of the plot of r^2 vs. t (Figure 7), the value of $\tilde{D}_i$ was calculated to be $4.33 \times 10^{-19}\ m^2s^{-1}$. This is very close to the value of "effective" interface diffusivity reported by Ardell and Ozolins [17], lying in between the reported diffusivity values in Ni [35] and Ni_3Al [36,37], suggesting that the process limiting coarsening as governed by an interface diffusion process could indeed be related to the Al diffusion through the order-disorder interface. Interestingly, Ardell and Ozolins [17] have pointed out that this interface diffusion model is the only one that accounts for the absence of dependence of coarsening kinetics on the volume fraction of γ'. It is important to note that in the current study, the total volume fraction of γ' has been observed to be fairly constant (as measured by SEM and EFTEM studies), and could in principle account for the good match between experimental data and both models of coarsening. However, it is possible that the TIDC model may actually explain the coarsening behavior better in cases where there is a significant change in the volume fraction of the precipitates, and this aspect needs to be investigated in future studies. Despite these issues, the experimental coarsening data presented in this paper on Rene 88DT provides encouraging evidence for an interface diffusion controlled process to be actually operative in γ' coarsening in Ni-base superalloys, especially considering the fact that values for atomic fraction of solute in the γ and γ' phases used in the analysis and the width of the interface, have been determined with reasonable accuracy from experimental 3D atom probe studies.

Clearly, from the calculations discussed above, it is rather difficult to establish unequivocally the validity of either the LSW or TIDC coarsening models to explain coarsening kinetics of γ' precipitates in Rene 88DT. Further complications are introduced by the fact that unlike the

model binary Ni-Al or ternary Ni-Al-Cr alloys discussed in the previously published literature [12,15,17,30], Rene 88DT contains a large number of solute elements including the principal ones, Cr, Co, Al, Ti, and, Mo; consequently, the coarsening process might be controlled by a combination of diffusivities of multiple solute elements. Determination of a single rate-limiting diffusion coefficient might be challenging in such a situation. Nevertheless, based on the present results and their analysis, the possibility of existence of an interface diffusion-controlled coarsening cannot be ignored. The key factor that may help establish the applicability of either coarsening models is the value of the diffusivity of the solute through the interface ($\tilde{D}_i$) relative to that through the disordered γ matrix. The interface diffusivity in turn is expected to be critically dependent on the structure and composition of the interface including the extent of chemical ordering. Therefore, further studies are required in order to establish the structure and composition of these order-disorder interfaces at the ~~nanometer to the~~ atomic length scales [38]. In this context it is important to note that diffusivity of the solute through the interface is likely to be a rate-limiting step during coarsening provided the interface is between an ordered phase and a disordered phase. In the case where both the matrix and precipitate phases are disordered, it is less ~~un~~likely that diffusion through the interface would be rate-limiting in the coarsening process.

One of the interesting implications of the TIDC model is the possible dependence of several key terms such as interface energy (γ), effective interface diffusivity ($\tilde{D}_i$) and capillary length (l_γ) on the actual compositional width as well as the nature of ordering present in the interface. Recent studies of the γ/ γ' interface structure and chemistry, conducted by coupling 3DAP tomography and aberration-corrected high-resolution scanning TEM [38] suggest that the compositional gradient across the interface, equivalent to the compositional width, may not be constant but actually may depend upon factors such as aging time, cooling rate and size of the γ' precipitate. In addition, the details of the order-disorder transition from the $L1_2$ ordered γ' structure to the disordered *fcc* solid solution are also being investigated by coupling these two characterization techniques. Such detailed characterization of the structure and chemistry of the interface will be of immense importance in determining the role of interface-controlled diffusion in the coarsening process.

5. Summary and Conclusions

a. Rene88DT samples were subjected to varying cooling rates after a supersolvus treatment. The resultant microstructure ~~depended on~~ was strongly dependent on the cooling rate, with water quenched (WQ) samples showing a ~~mono~~uni modal γ' size and slow cooled (SC) and fast cooled (FC) samples showing a bimodal γ' size distribution.

b. The experimentally-determined coarsening data for γ' precipitates in Rene88DT (aging at 760^{0}C) ~~has been fitted~~ was fit to both the classical LSW model (r^3 vs. t), based on solute diffusion through the matrix, and the trans-interface diffusion controlled (TIDC) coarsening model (r^2 vs. t) based on interface diffusion-controlled coarsening. Coarsening rate constants ~~have been~~ were calculated for selected size ranges of γ' precipitates that retain equilibrium shapes and ~~are~~ were near-spherical (size < 25nm). The experimentally determined coarsening data fits the LSW (r^3 vs. t) ~~as well as the~~ and TIDC (r^2 vs. t) models equally well.

Isn't size a factor of the previous two (t, cooling rate) + T

Is it unimodal or monomodal? You need both in this paper.

c. In case of the LSW model, the coarsening rate constant was calculated analytically using values for ~~certain~~ parameters from 3D atom probe experiments (such as compositions of the γ and γ' phases) ~~as well as some~~ from the literature (such as the interfacial energy γ). Possible rate limiting steps, involving the diffusion of Al or Cr in Ni, yielded good agreement between the analytically derived rate constant and the experimentally determined value.

d. In case of the TIDC model, the experimentally determined coarsening rate constant was used to compute the effective interface diffusivity based on an analytical expression for the coarsening rate constant. The value of $\tilde{D}_i$ ~~is~~ 4.33×10^{-19} $m^2 s^{-1}$, which lies ~~in~~ between the inter-diffusivity values for Al in Ni and Al in Ni_3Al. This suggests that the γ/γ' interface is possibly partially ordered, and consequently diffusion of solute through the interface could act as a rate-limiting step for coarsening.

Acknowledgements:

This work was conducted as part of the joint research of the Alloy Development Group of the Air Force Research Laboratory's Materials and Manufacturing Directorate, The Ohio State University Materials Science and Engineering Department, and the Materials Department at the University of North Texas. The work was partly funded by the Air Force Office of Scientific Research under the management of Dr. Joan Fuller. Additional support was provided by Mr. Kevin Shively and Mr. Bob Lewis at the Air Force Research Laboratory, and Dr. John Gayda, at the NASA Glenn Research Center. The support and facilities from the Center for the Accelerated Maturation of Materials (CAMM) at the Ohio State University and the Center for Advanced Research and Technology (CART) at the University of North Texas are gratefully acknowledged.

References:

1. Reed, R.C. in *The Superalloys, Fundamentals and Applications*, Cambridge University Press, 236-257 (2006).
2. Telesman, J., Kantzos, P., Gayda, J., Bonacuse, P.J., Prescenzi, A., Microstructural Variables Controlling Time-Dependent Crack Growth in a P/M Superalloy, in *Superalloys 2004,* ed. Green, K.A. et al., TMS Publications, Warrendale, PA, 215-224 (2004).
3. Gabb, T., et al., Phase Stability of a Powder Metallurgy Disk Superalloy, Technical Presentation, NASA Glenn Research Center, October 2006.
4. Sondhi, S.K., Dyson, B.F., and McLean, M., Acta Materialla **52**, 1761-1772 (2004).
5. Fahrmann, M., Hermann, W., Fahrmann, E., Boegli, A., Pollock, T.M., Sockel, H.G., Materials Science and Engineering, **A271**, 122-127 (1999).
6. Gornostyrev, Yu.N., Kontsevoi, O.Yu., Khromov, K.Yu., Katsnelson, M.I., Freeman, A.J., Scripta Materialia **56**, 81-84 (2007).
7. Viswanathan, G.B., Sarosi, P.M., Henry, M.F., Whitis, D.D., Milligan, W.W., Mills, M.J., Acta Mater **53**, 3041-3057 (2005).
8. Sarosi, P.M., Viswanathan, G.B., Whitis, D., Mills, M.J., Ultramicroscopy, **103**, 83-93 (2005).
9. Lifshitz, I.M., Slyozov, V.V., J. Phys. Chem. Solids, **19**, 35-50 (1961).
10. Wagner, C., Z. Elektrochem., **65**, 581-591 (1961).
11. Ardell, A.J., Acta metall., **20**, 61-71 (1972).
12. Chellman, D.J., Ardell, A.J., Acta metall., **22**, 577-587 (1974).
13. Ardell, A.J., Nicholson, R.B., J. Phys. Chem. Solids, **27**, 1793-1804 (1966).
14. Voorhees, P.W., J. Stat. Phys. **38**, 231–252 (1985).
15. McLean, D., Metal Sci., **18**, 249-256 (1984).
16. Ratke, L., Voorhees, P.W., in *Growth and Coarsening*, Springer: Berlin (2002).
17. Ardell, A.J., Ozolins, V., Nature Materials, **4**, 309-316 (2005).
18. Littles, Jr., J.W., Pettit, R.G., Schirra, J.J., Cowles, B.A., Holmes, R.A., Russ, S.M., Rosenberger, H., Larsen, J.M., in *Materials Damage Prognosis*, TMS Publications, Warrendale, PA, 23-29 (2005).
19. Fovea Pro® Software, Reindeer Graphics (2003).
20. Adobe® Photoshop CS2, Version 9.0, Adobe Systems Incorporated (2005).
21. Searles, T., Tiley, J., Tanner, A., Williams, R., Rollins, B., Lee, E., Kar, S., Banerjee, R., Fraser, H.L., Measurement Science and Technology, **16**, 60-69 (2005).
22. Tiley, J., Searles, T., Lee, E., Kar, S., Banerjee, R., Russ, J.C., Fraser, H.L., Materials Science and Engineering A, **372**, 191-198 (2004).
23. Hwang, J., Banerjee, R., Tiley, J., Srinivasan, R., Viswanathan, G.B., Fraser, H.L., submitted to Mater. Trans.A (2008).
24. Wlodeck, S.T., Kelly, M., Alden, D.A., in *Superalloys 1996*, ed. Kissinger, R.D., Deye, D.J., et al., TMS Publications, Warrendale, PA, 129 (1996).
25. Safari, J., Nategh, S., and McLean, M. Mater. Sci. Technol. **22**, 888-898 (2006).
26. Parratt, L., Probability & Experimental Errors in Science; An Elemental Survey, Wiley Publishers (1966).
27. Tiley, J., Viswanathan, G.B., Srinivasan, R., Banerjee, R., Fraser, H.L., manuscript under preparation (2008).
28. Hellman, O.C., Vandenbroucke, J.A., Rüsing, J.,Isheim, D., Seidman, D.N., Micros. Microanal., **6**, 437-444 (2000).

29. Sudbrack, C.K., Ph.D. Thesis, Northwestern University (2004).
30. Calderon, J.A., et al., Acta Metall. Mater. **42**, 991-1000 (1994).
31. Baldan, A., J. Mater. Sci. **37**, 2379 (2002).
32. Swalin, R.A., and Martin, A., J. Metals, **8**, 576 (1956).
33. Isheim, D., Hsieh, G., Noebe, R.D., Seidman, D.N., in *Solid-to-Solid Phase Trans. Inorg. Mater., Vol I: Diffusional Transformations*, ed. Howe, J.M., Laughlin, D.E., Lee, J.K., Dahmen, U. and Soffa, W.A., TMS Publications, Warrendale, PA (2005).
34. Smithell's Handbook 7th edn, ed. Brandes, E.A., Brook, G.B., Butterworth-Heinemann, Oxford, UK (1992).
35. Janssen, M.M.P, Metall. Trans. **4**, 1623 (1973).
36. Fujiwara, K., Horita, Z., Acta Mater. **50**, 1571-1579 (2002)
37. Ikeda, T., Almazouzi, A., Numakura, H., Koiwa, M., Sprengel, W., Nakajima, H., Acta Mater. **46**, 5369 (1998).
38. Srinivasan, R., Banerjee, R., Hwang, J.Y., Viswanathan, G.B., Tiley, J., Dimiduk, D.M. and Fraser, H.L., submitted to *Nature Materials*.

Table and Figure Captions

Table 1: Bulk Chemical Composition for Rene88DT (all values in weight %)

Table 2: Calculated rate constants for various starting conditions (cooling rates) in Rene88DT, based upon the fit to the LSW [9,10] model.

Table 3: Calculated rate constants for various starting conditions (cooling rates) in Rene88DT, based upon the fit to the Ardell and Ozolins [17] model.

Figure 1: EFTEM micrographs from samples subjected to different cooling rates *prior to aging*: (a) WQ, (b) FC (c) SC samples.

Figure 2: EFTEM micrographs from samples subjected to different cooling rates, followed by *aging for 200 hours at* 760^0C (a) WQ (b) FC (c) SC samples.

Figure 3: Equivalent diameter size plot showing the evolution in size of γ' precipitates as a function of aging time at 760^0C, for different cooling rates. For FC and SC samples, the size evolution of "tertiary" γ' precipitates is shown.

Figure 4: 3D atom probe tomography results from the Rene 88DT sample, water-quenched followed by aging at 760°C for 50 hours. (a) 3D reconstruction of iso-concentration surface at Al = 8at% in red and Co atoms in blue. (b) 3D reconstruction of iso-concentration surface at Cr = 14at%. (c) Compositional profile in the form of a proximity histogram for the primary alloying elements, Cr, Co, Mo, Al, and, Ti in Rene 88DT. The compositional width of the interface, determined from consideration of the Cr compositional gradient across it, has been marked.

Figure 5: EFTEM micrographs showing the large (secondary) and small (tertiary) γ' precipitates in SC samples aged to (a) 100 and (b) 200 hours respectively. Specific instances of splitting of very coarse secondary γ' particles are shown in (b).

Figure 6: Plot of precipitate size (r^3) vs. aging time (t) during aging at 760^0C for different microstructures. Best linear fits with the three data sets are shown, together with the appropriate functional relationship between r^3 and t, from which the rate constants are deduced. These rate constants are also shown.

Figure 7: Plot of precipitate size (r^2) vs. aging time (t) during aging at 760^0C for different microstructures. Best linear fits with the three data sets are shown, together with the appropriate functional relationship between r^2 and t, from which the rate constants are deduced. These rate constants are also shown.

	Al	Ti	Cr	Co	Nb	Mo	W	C	B	Ni
Average (wt%)	1.77	4.05	16.01	13.02	0.70	3.98	4.07	0.049	<0.03	Bal.

Table 1: Bulk Chemical Composition for Rene88DT

Cooling condition (cooling rate)	**k, nm^3s^{-1}**	**Coefficient of Determination (R^2)**
Water Quenched secondary (>300^{0}C/min)	0.0157	0.976
Fast Cooled tertiary (280^{0}C/min)	0.0049	0.973
Slow Cooled tertiary (24^{0}C/min)	0.0057	0.936

Table 2: Calculated rate constants for various starting conditions (cooling rates) in Rene88DT, based upon the fit to the LSW [9,10] model.

Cooling Condition (Cooling rate)	k, nm^2s^{-1}	Coefficient of Determination (R^2)
Water Quenched secondary (>300^{0}C/min)	0.0006	0.983
Fast Cooled tertiary (280^{0}C/min)	0.0003	0.969
Slow Cooled tertiary (24^{0}C/min)	0.0003	0.875

Table 3: Calculated rate constants for various starting conditions (cooling rates) in Rene88DT, based upon the fit to the Ardell and Ozolins [17] model.

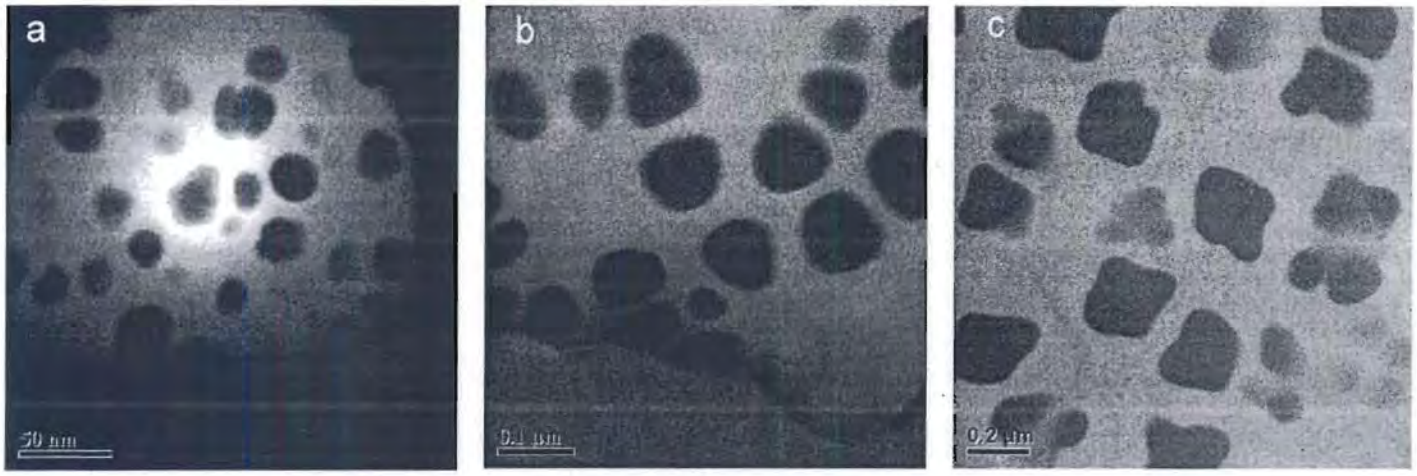

Figure 1: EFTEM micrographs from samples subjected to different cooling rates *prior to aging*: (a) WQ, b) FC (280^0C/min), c) SC (24^0C/min) samples.

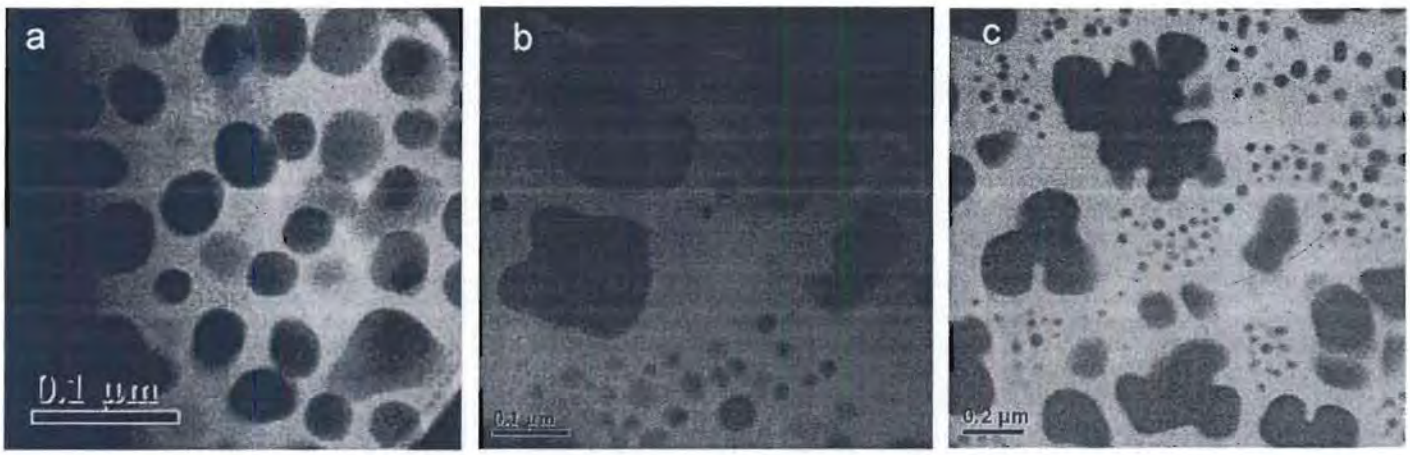

Figure 2: EFTEM micrographs from samples subjected to different cooling rates, followed by *aging for 200 hours at* 760^0C (a) WQ (b) FC (c) SC samples.

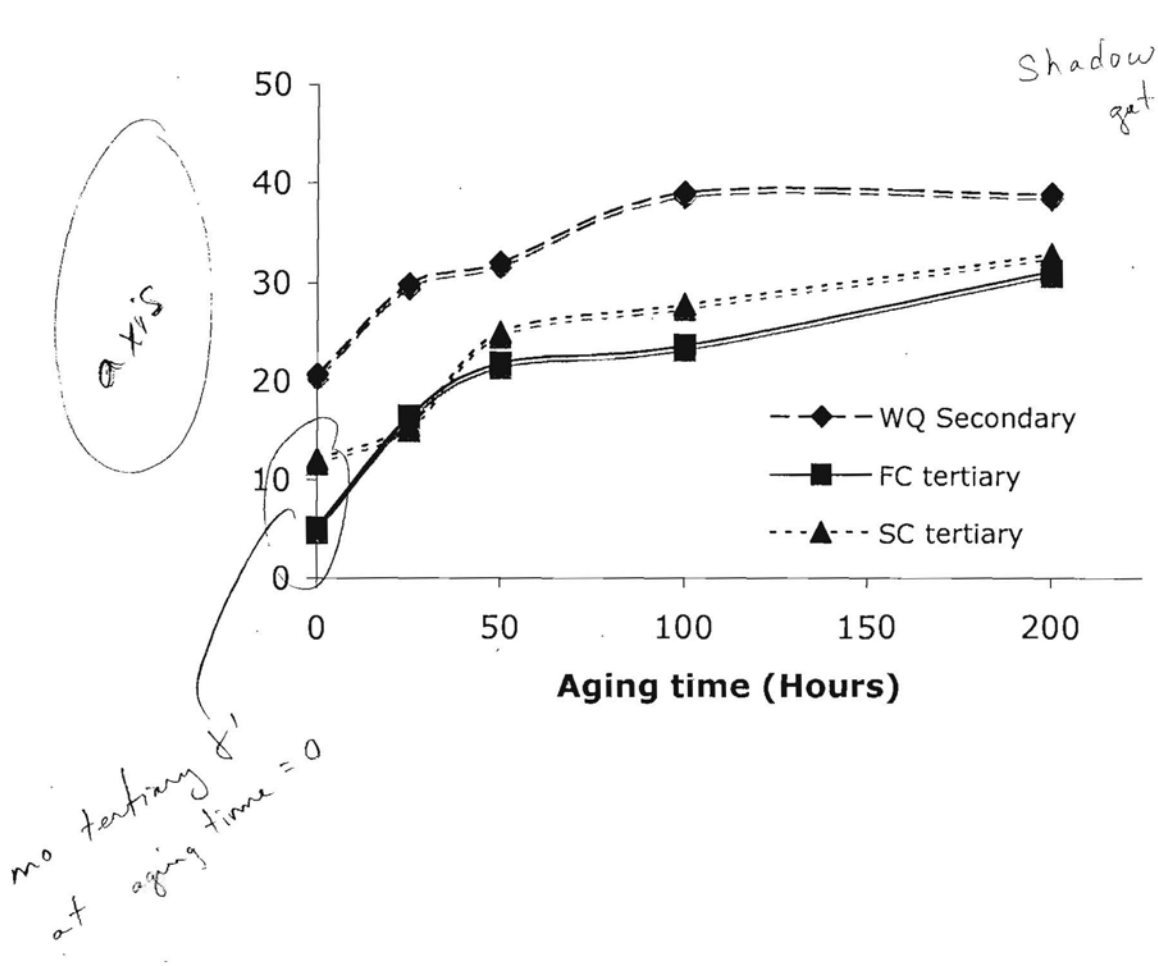

Figure 3: Equivalent diameter size plot showing evolution in sizes of γ' precipitates as a function of aging time at 760^{0}C, for different cooling rates. For FC and SC samples, the size evolution of "tertiary" γ' precipitates is shown.

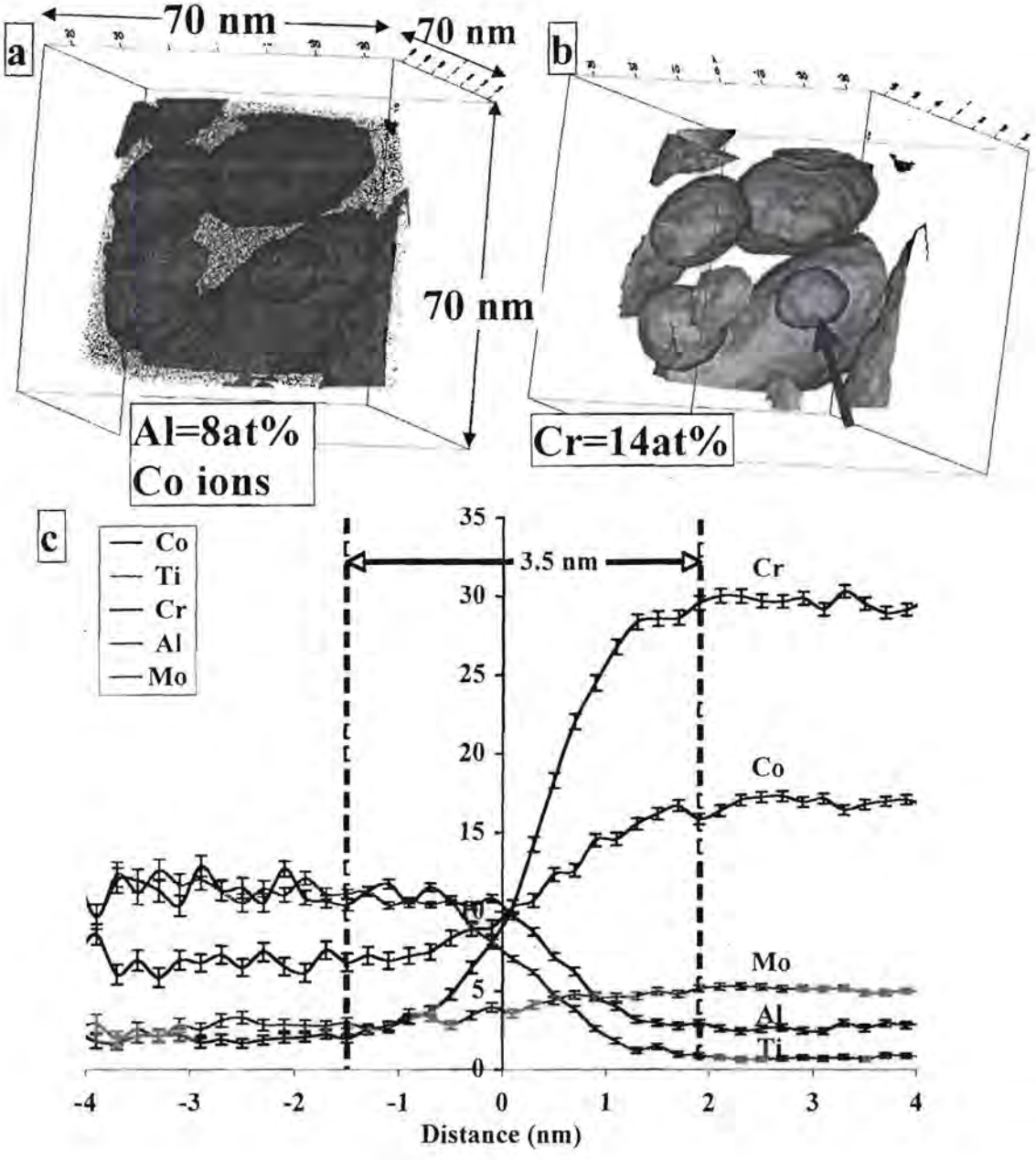

Figure 4: 3D atom probe tomography results from the Rene 88DT sample, water-quenched followed by aging at 760°C for 50 hours. (a) 3D reconstruction of iso-concentration surface at Al = 8at% in red and Co atoms in blue. (b) 3D reconstruction of iso-concentration surface at Cr = 14at%. (c) Compositional profile in the form of a proximity histogram for the primary alloying elements, Cr, Co, Mo, Al, and, Ti in Rene 88DT. The compositional width of the interface, determined from consideration of the Cr compositional gradient across it, has been marked.

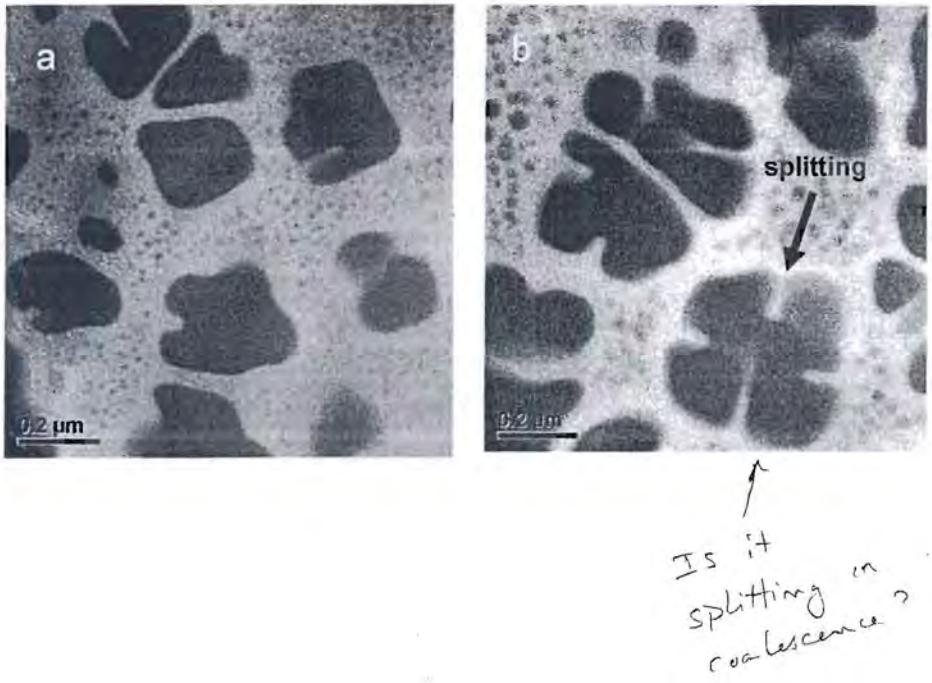

Figure 5: EFTEM micrographs showing the large (secondary) and small (tertiary) γ' precipitates in SC samples aged to (a) 100 and (b) 200 hours respectively. Specific instances of splitting of very coarse secondary γ' particles are shown in (b).

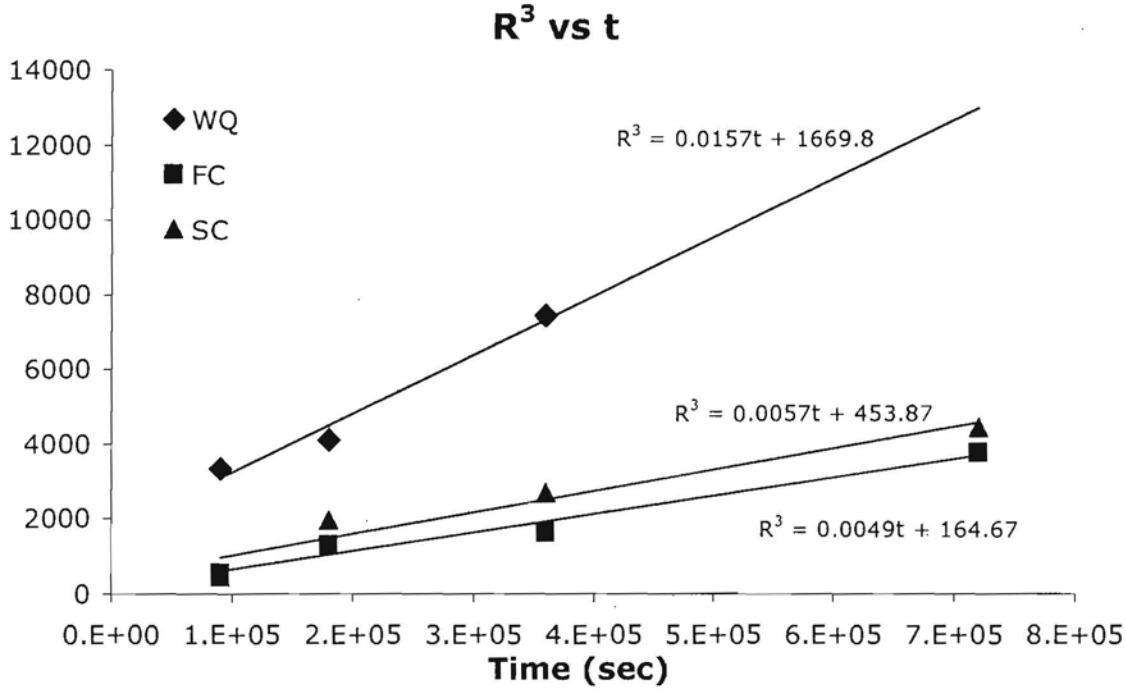

Figure 6: Plot of precipitate size (r^3) vs. aging time (t) during aging at 760^0C for different microstructures. Best linear fits with the three data sets are shown, together with the appropriate functional relationship between r^3 and t, from which the rate constants are deduced. These rate constants are also shown.

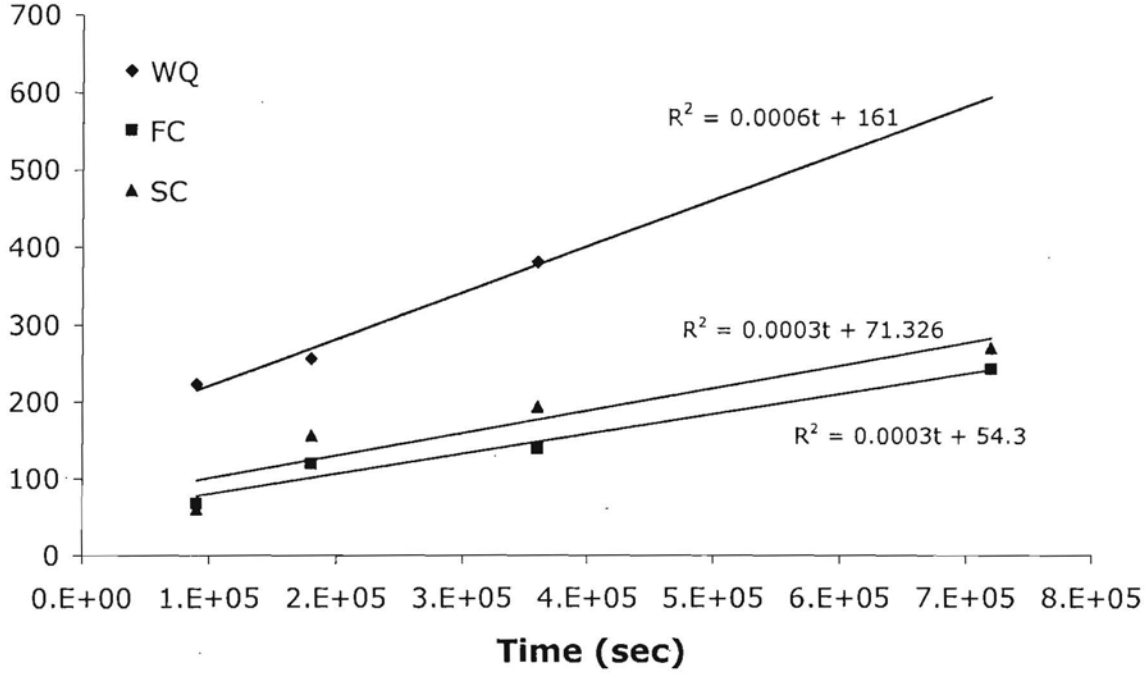

Figure 7: Plot of precipitate size (r^2) vs. aging time (t) during aging at 760^0C for different microstructures. Best linear fits with the three data sets are shown, together with the appropriate functional relationship between r^2 and t, from which the rate constants are deduced. These rate constants are also shown.